PLANETARY SCIENCE

A unique stone skipping–like trajectory of asteroid Aletai

Ye Li[1,2]*†, Bin Li[1,2]†, Weibiao Hsu[1,2]*, A. J. Timothy Jull[3,4], Shiyong Liao[1,2], Yuhui Zhao[1,2], Haibin Zhao[1,2], Yunhua Wu[5], Shaolin Li[6], Chipui Tang[6]

Meteoroids/asteroids could deposit energy to Earth during their entries, which arouses great concerns. Strewn field, as a product of meteoroids/asteroids breakup, comprehensively reflects the trajectory, dynamics, and physical properties of meteoroids/asteroids. It typically has a length of several to a dozen kilometers. Nevertheless, the recently found massive Aletai irons in the northwest China comprise the longest known strewn field of ~430 kilometers. This implies that the dynamics of Aletai could be unique. Petrographic and trace elemental studies suggest that all the Aletai masses exhibit unique compositions (IIIE anomalous), indicating that they were from the same fall event. Numerical modeling suggests that the stone skipping–like trajectory associated with a shallow entry angle (e.g., ~6.5° to 7.3°) is responsible for Aletai's exceptionally long strewn field if a single-body entry scenario is considered. The stone skipping–like trajectory would not result in the deposition of large impact energy on the ground but may lead to the dissipation of energy during its extremely long-distance flight.

INTRODUCTION

Meteoroids/asteroids invade the Earth's atmosphere at varying entry angles (from <5° to near-vertical angle) and velocities (~11 to 70 km/s), break apart into fragments in the atmosphere, fall as meteorite showers, and create funnels and craters (*1*–*3*). During this process, meteoroids/asteroids could deposit large amounts of kinetic energy, and some asteroids may result in severe explosions or even affect the ecosystem (*4*, *5*). Thus, it is crucial to understand how the meteoroids/asteroids fall through the atmosphere. Strewn field, as a product of meteoroids/asteroids breakup during flight or impact, consists of dispersed meteorites on the ground. It comprehensively reflects the trajectory, dynamics (e.g., entry angle and velocity) and physical properties (e.g., internal structure, shape, and density) of meteoroids/asteroids (*6*, *7*). The length of a strewn field is typically in a range of several to a dozen kilometers. Longer strewn fields could exist [e.g., asteroid 2008 TC3 with a 30-km-long strewn field (*8*)], but those as long as 40 km or above are rather rare.

The recently reported massive Aletai irons were recovered in the Aletai region, northwest of Xinjiang Province, China, and close to the China-Mongolia border (Fig. 1). Up to now, their total weight is over 74 tons with five main masses (details about the recovery of Aletai irons shown in Supplementary Text). A 23-ton WuQilike (48°02.28′N, 88°23.05′E, newly found in 2021 and updated in Meteoritical Bulletin 110 online; www.lpi.usra.edu/meteor/metbull.php), 18-ton Akebulake (48°06.25′N, 88°16.57′E) (*9*), 5-ton Wuxilike (48°03.13′N, 88°22.32′E) (*10*), and two other relatively small masses [35-kg Xinjiang(b) and 15-kg unnamed iron] are concentrated near Xiaodonggou area with a total mass over 46 tons. The largest single mass 28-ton Armanty (Dongte Village, Agasheaobao Town, Qinghe County; 45°52.27′N, 90°30.28′E) (*11*, *12*) and 0.43-ton Ulasitai (Beita Mountain, Mulei County, 44°57.40′N, 91°24.15′E) are ~310 and ~430 km away from Xiaodonggou area, respectively (Fig. 1) (*13*). No contemporary impact craters are observed in the vicinity (see Discussion for more details). The fact that the five main masses (~0.43 to 28 tons) are so large indicates that most of the Aletai irons, if not all, were found at or quite close to their original fall sites. The recovery sites of the irons are located geographically on an array with a length of ~430 km, extending from southeast to northwest (Fig. 1). Detailed petrographic and geochemical analyses of Armanty, Ulasitai, and Wuxilike revealed essentially the same internal texture and trace element contents, indicating that they are likely paired and belong to the same fall (*10*, *13*). If this is the case, then the length of the strewn field of Aletai (~430 km) outdistances that of Campo del Cielo (~18.5 km), which is comparably composed of several large irons (e.g., 37.4-ton El Chaco, ~30-ton El Gancedo, and 15-ton Meson de Fierro) (*14*, *15*). Furthermore, it is also much longer than that of Gibeon (a long axis of 275 km, not entirely convincing due to the possible displacement of masses) (*16*), becoming the longest strewn field on Earth (*10*). The extraordinary long strewn field implies that the trajectory and/or dynamics of asteroid Aletai are unique.

In this work, a comprehensive study of petrology, whole-rock trace element geochemistry, together with radionuclide analyses and numerical modeling was carried out for Aletai irons. The results show that a 430-km-long strewn field could be generated if asteroid Aletai entered Earth's atmosphere at a shallow angle and traveled along a unique stone skipping–like trajectory. Our study provides deep insights into the formation mechanism of a long strewn field in the nature.

RESULTS

Petrographic study of Akebulake and WuQilike

Petrographic studies have previously been conducted for some large masses, such as Armanty, Wuxilike, and Ulasitai (*10*, *11*, *13*, *17*). Here, we perform detailed petrographic and mineralogical studies

[1]Purple Mountain Observatory, Chinese Academy of Sciences, Nanjing 210023, China. [2]CAS Center for Excellence in Comparative Planetology, Hefei, China. [3]Department of Geosciences, University of Arizona, Tucson, AZ 86721, USA. [4]Isotope Climatology and Environmental Research Centre, Institute for Nuclear Research, Debrecen, Hungary. [5]Planetary Environmental and Astrobiological Research Laboratory, School of Atmospheric Sciences, Sun Yat-sen University, Zhuhai 519082, China. [6]State Key Laboratory of Lunar and Planetary Sciences, Macau University of Science and Technology, Avenida Wai Long, Taipa, Macau.
*Corresponding author. Email: liye@pmo.ac.cn (Y.L.); wbxu@pmo.ac.cn (W.H.)
†These authors contributed equally to this work and are co–first authors.

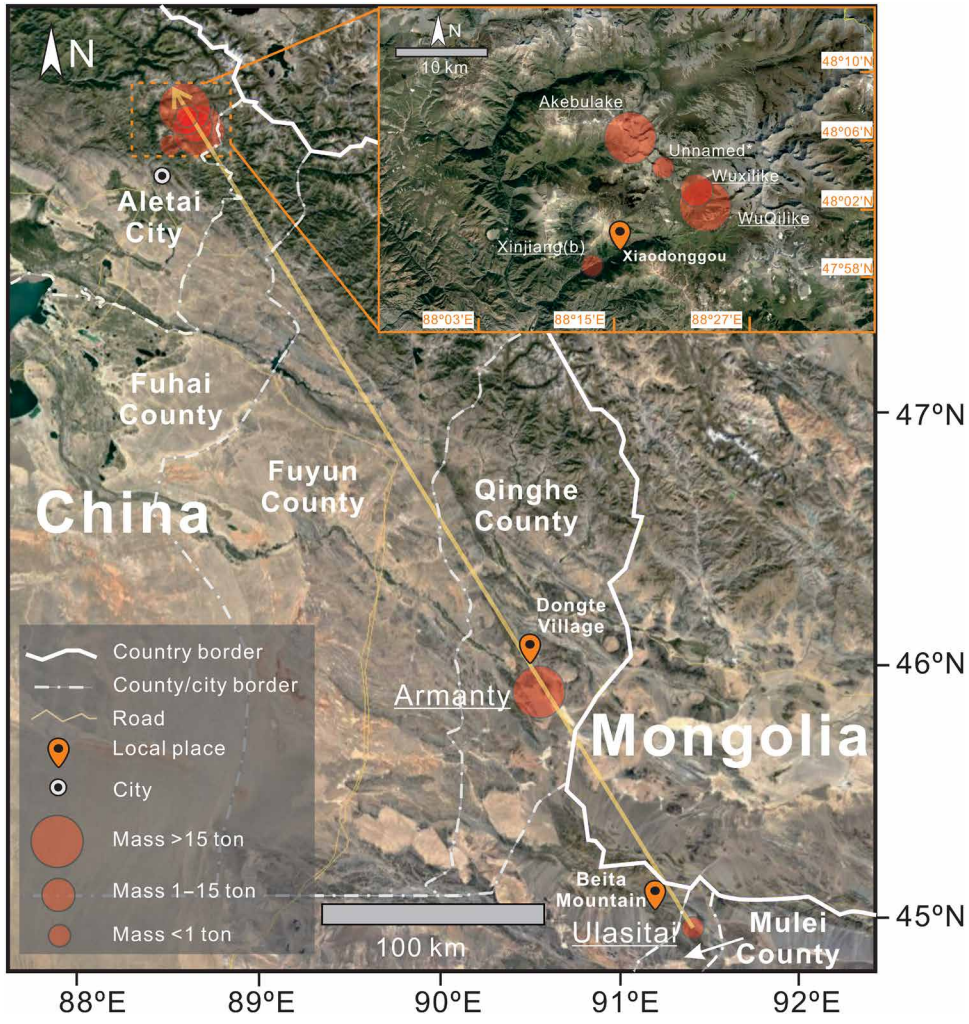

Fig. 1. Map of the recovery sites of Aletai masses. The close-up of recovery sites in Xiaodonggou area shown in the top right corner. Only the masses listed in the Meteoritical Bulletin (www.lpi.usra.edu/meteor/metbull.php) are plotted. The base map is from Google Earth. Asterisk denotes the unnamed 15 kg of mass that was found in the Xiaodonggou area close to Wuxilike and Akebulake without precise latitude and longitude. We plot it in the middle between Wuxilike and Akebulake.

for Akebulake and WuQilike. Akebulake and WuQilike consist mainly of kamacite (~80 to 83 volume %), taenite (~10 to 11 volume %), plessite (~3 to 8 volume %), and schreibersite (~2 to 3 volume %) with minor troilite, haxonite, and daubréelite (table S1). Kamacite plates [7.0 ± 0.1 weight % (wt %) Ni for both] display a medium-sized Widmanstätten pattern with a bandwidth of ~1 to 1.4 mm (table S1). The primary cooling rates of Akebulake and WuQilike are estimated to be over ~10°C/million years (Ma) to 40°C/Ma based on the method from Wood (*18*)(fig. S1). Similar to most of the masses (*10*, *13*, *19*), the newly found WuQilike contains few shock features; nevertheless, Akebulake is moderately to strongly shocked based on the occurrence of extensive remelting of sulfide and phosphide and a large degree of haxonite decomposition (see Supplementary Text and fig. S2 for more details). The petrography and mineralogy of Akebulake and WuQilike are summarized in table S1, along with the literature data of Wuxilike, Ulasitai, and Armanty for comparison (*10*, *11*, *13*, *17*, *20*). Representative mineral compositions of WuQilike and Akebulake are given in tables S2 and S3, respectively.

Whole-rock compositions

The preliminary bulk instrumental neutron activation analysis (INAA) data of Aletai irons were reported in Meteoritical Bulletin 105 (*9*). Four large Aletai irons, including Armanty, Akebulake, Wuxilike, and Ulasitai, were reanalyzed by using a technique of improved integration of gamma-ray peaks (see Materials and Methods for more details) (*21*, *22*). They have indistinguishable contents of selected elements (table S4). We plot Co, Ga, and Ir versus Au content for Aletai irons along with IIIAB and IIIE irons for comparison (Fig. 2). On the plots, Co and Au contents of Aletai are much higher than the other IIIE irons (Fig. 2A). The plotting of Aletai irons follows the extension of Au-Ga and Au-Co trend line of IIIE irons (Fig. 2, A and B) but is out of the range of the extension of IIIE Au-Ir trend line (Fig. 2C).

Radionuclide contents and the initial mass

Wuxilike and Akebulake show low levels of ^{10}Be (0.03 to 0.39 dpm/kg; table S5), compatible with the results from other large irons such as

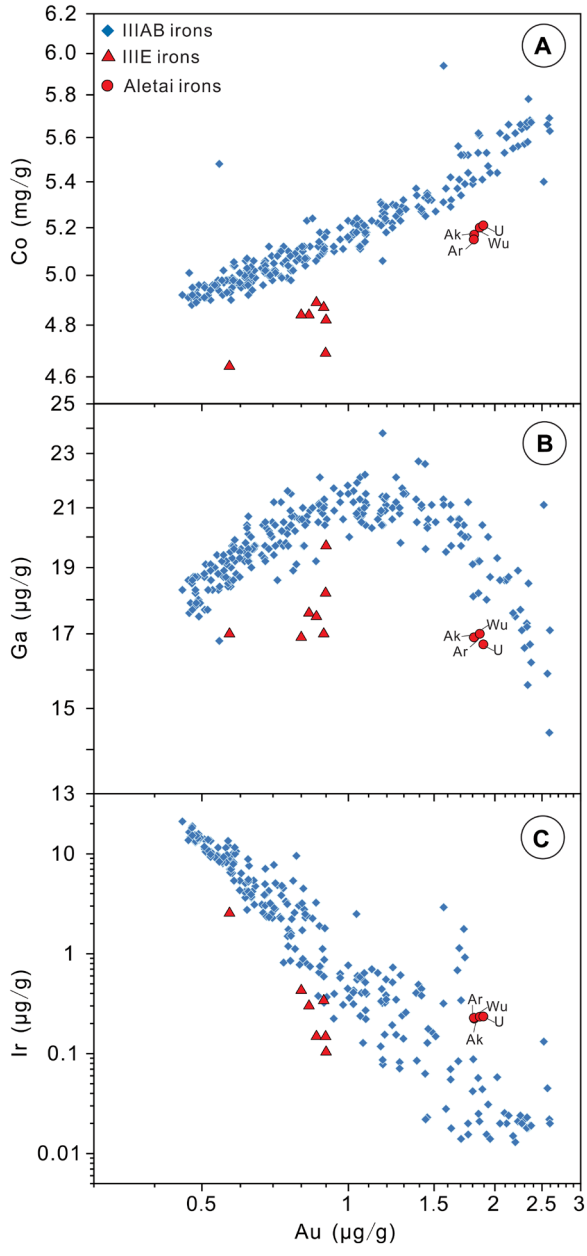

Fig. 2. Trace elements versus Au for Aletai irons. Aletai data from this study, and IIIE and IIIAB data for comparison. IIIAB data from Chabot and Zhang (*55*). IIIE data from Malvin *et al.* (*27*) and online Meteoritical Bulletin Database (www.lpi.usra.edu/meteor/metbull.php). U, Ulasitai; Wu, Wuxilike; Ak, Akebulake; Ar, Armanty.

Gibeon (0.09 to 0.58 dpm/kg) (*23*, *24*). Assuming that the density is about 7800 kg/m^3 and the production rate of ^{10}Be near the surface of iron is ~6 dpm/kg (*23*), the estimated buried depth is about 56 cm for Wuxilike and 108 cm for Akebulake. This suggests that Wuxilike would be at a relatively shallow depth. A buried depth of ~108 cm (±10 cm) for Akebulake implies that the radius of the pre-atmospheric object is at least ~108 cm. This is roughly compatible with the lower limit of the estimated radius for Armanty (~130 to 160 cm) within analytical uncertainties (*25*). Nevertheless, an initial mass of 31 to 54 tons derived from a radius of ~98 to 118 cm is apparently lower than the total mass of Aletai currently recovered (>74 tons). An initial mass of 70 to 135 tons was estimated on the basis of the noble gas study of Armanty (*25*). This mass is generally compatible with the total mass of Aletai currently recovered but seems to be largely underestimated if the inevitable mass loss during the entrance is considered. A larger initial mass (e.g., >200 tons) is more realistic for the asteroid Aletai.

Numerical modeling

The northwest end of this strewn field (within a range of ~10 km) is characterized by the occurrence of several large masses (5 to 23 tons) and a concentration of more than half of the total mass (46 of 74 tons). This indicates that (i) the flying direction of Aletai is from southeast to northwest (Fig. 1; see Discussion for more details) and that (ii) Aletai seems to have experienced disintegration(s) near the northwest end. The dynamics of Aletai is tested by assuming a single-body entry in the atmosphere. The details of modeling are described in Materials and Methods.

We use the Monte Carlo method to get a general view of the dynamics. Three basic input parameters are initial velocity (11.2 to 20 km/s), initial mass (200 to 20,000 tons), and entry angle (4° to 10°). In the entry angle versus initial velocity plotting (Fig. 3A), samples with different trajectories are marked by different colors. Among them, the stone skipping–like trajectory is defined to describe the flight path of sample cases in which at least one fragment flies with a bounce and fall in Earth's atmosphere. The red "stone skipping–like trajectory zone," confined between the blue "grazing zone" and gray "direct falling zone," shows a positive correlation between initial velocity and entry angle (Fig. 3A). A relatively low entry angle (~6° to 8°) is essential for the formation of a strewn field longer than 150 km (Fig. 3B). In contrast, a higher (>8°) or lower (<6°) entry angle would lead to a relatively short strewn field or earth-grazers. In all the samples involving the length of strewn field over 430 km, 96% samples have a stone skipping–like trajectory. Thus, the stone skipping–like trajectory seems to be necessary to yield a strewn field with a length over 430 km (Fig. 3B). On the basis of the current understanding of Aletai strewn field, the trajectory of Aletai with corresponding dynamics is explored by Markov chain Monte Carlo (MCMC) method. We give several constraints for the modeling parameters: (i) the longest distance between large fragments (individual mass > 20 tons) of 300 km (σ = 50), (ii) the maximum weight of final single fragment of 50 tons (σ = 10), and (iii) the number of large masses (individual mass > 20 tons) of 2 (see Materials and Methods for more details). Our results show that asteroid Aletai has an initial velocity of ~11.9 to 14.9 km/s, entry angle of ~6.5° to 7.3°, and initial mass of ~280 to 3440 tons with a radius of ~2.1 to 4.7 m (99% credible bounds; fig. S3 and table S6). The corresponding final impact velocity and impact energy are relatively low with an impact angle of 19° to 26° (~0.6 to 0.9 km/s and ~1 to 8 t trinitrotolune (TNT) for the largest final mass; table S7). There is a trend that the larger mass is present in the farther end. The MCMC samples show that the total length of the strewn field (assumed equivalent to the longest distance between fragments with individual mass over 0.5 tons) is mainly between 300 and 800 km with a few over 1000 km (table S7). The detailed sketches of trajectory and changes of dynamic pressure were exported from 50 randomly selected cases and show that the dynamic pressure at breakup is about ~3 to 4 MPa. One of the representative cases is given in Fig. 4 and fig. S4 with a summary of parameters in table S8.

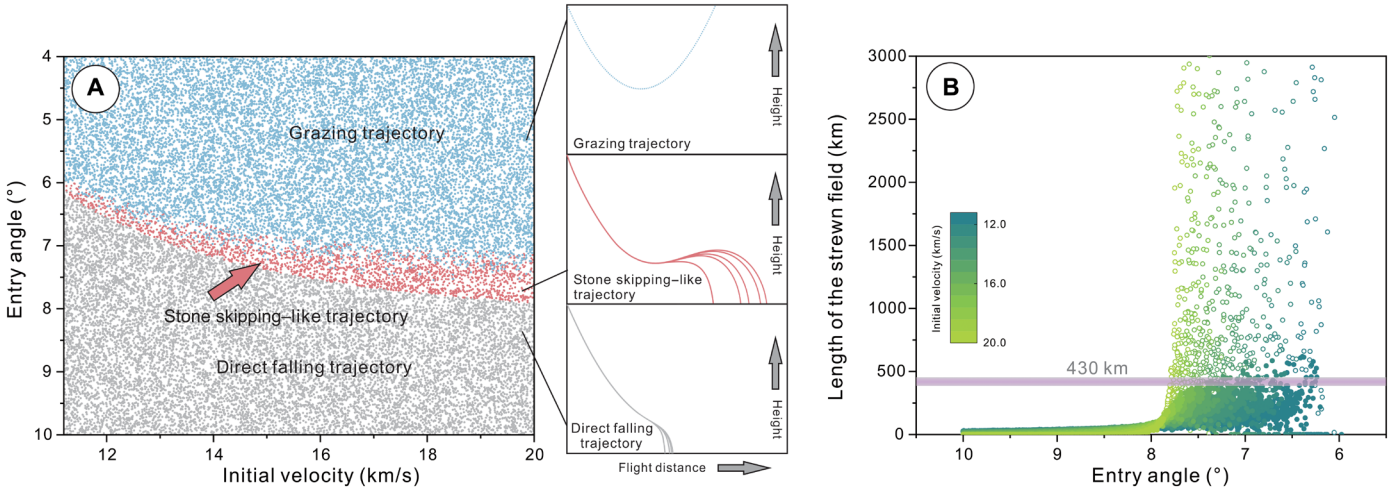

Fig. 3. MC modeling results for asteroid Aletai. The entry angle versus initial velocity plotting (**A**) and length of the strewn field versus entry angle plotting (**B**) based on the Monte Carlo method. In (A), the gray spots refer to the samples with direct falling trajectory, the red spots refer to the samples with stone skipping–like trajectory, and the blue spots refer to the samples as earth's grazers. The schematic trajectory diagrams from Monte Carlo modeling are shown to the right. In (B), the open circles refer to the samples with a stone skipping–like trajectory, and the solid circles refer to the direct falling objects. The length of strewn field is assumed to be equivalent to the longest distance between fragments weighing over 0.5 tons individually. Panel (B) only shows the samples with length of strewn field less than 3000 km; there are also a few samples with length over 3000 km.

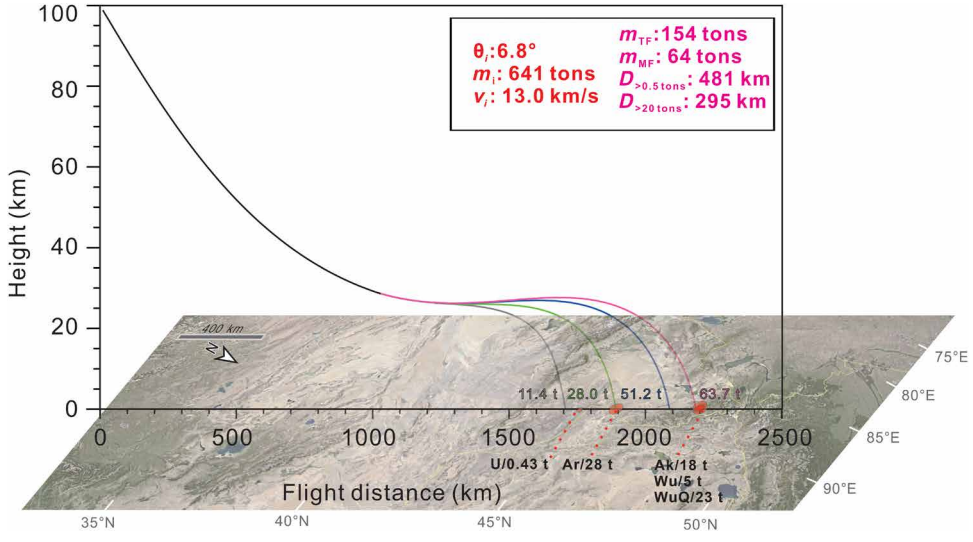

Fig. 4. A representative trajectory motion of asteroid Aletai. The numbers above the *x* axis refer to the computed weight of final masses, and only the fragments with weight over 0.5 tons are shown here. The currently known Aletai masses are marked by red ellipses along the *x* axis. The corresponding dynamic pressure variations are shown in fig. S4. θ_i = entry angle, m_i = initial mass, v_i = initial velocity, m_{TF} = the weight of total final fragments, m_{MF} = the weight of the largest final fragment, $D_{>0.5\,tons}$ = the longest distance between fragments with individual weight over 0.5 tons (assumed to be equal to the length of the strewn field), $D_{>20\,tons}$ = the longest distance between fragments with individual weight over 20 tons, and WuQ = WuQilike. The other abbreviations are the same as those in Fig. 2. The base map is from Google Earth.

DISCUSSION

Akebulake, WuQilike, and other Aletai masses share a great similarity in mineral chemistry (e.g., ~5.5 to 7.0 wt % Ni in kamacite), kamacite bandwidth of ~1.0 to 1.4 mm, mineral modal abundances, and primary cooling rate (>10°C/Ma to 40°C/Ma; table S1). All the analyzed masses essentially have identical bulk compositions (Fig. 2 and table S4). This suggests that all Aletai masses are paired. Although varying degrees of shock metamorphism are shown between different masses, it could result from the uneven distribution of heat and kinetic energy during impact on Aletai's parent body. IIIE is a small iron meteorite group, consisting of only 16 members. Group IIIE irons are chemically similar to IIIAB irons but can be distinguished from IIIAB irons based on (i) the occurrence of haxonite or graphite (from the decomposition of haxonite during shock) in plessite (*26*), (ii) relatively low Ga/Ni and Ge/Ni ratios on element-Ni diagrams (e.g., Co-Ni and Ga-Ni diagrams) (*27*), and (iii) relatively coarse kamacite bandwidths (~1.3 to 1.5 mm for IIIE irons versus ~0.5 to 1.4 for IIIAB irons) (*26*). Comparable with typical IIIE irons, all the Aletai masses are characterized by the presence of haxonite and relatively coarse kamacite bandwidth (~1.0 to 1.4 mm). Previous

studies of Armanty, Ulasitai, and Wuxilike masses suggested that Aletai belongs to IIIE irons based on the element-Ni diagrams (*10*, *13*, *27*). A better resolution can be made if Au is used as an independent variable rather than Ni (*28*). Different from other IIIE members, Aletai irons are characterized by (i) higher Au and Co contents and (ii) unexcepted Ir contents that do not fall on extrapolation of the Au-Ir trend of the other IIIE irons. Overall, by combining geochemical data with petrologic observations, we concur with the conclusion of Meteoritical Bulletin 105 (*9*) that Aletai is an anomalous IIIE iron. The composition of Aletai irons is so unique that no other samples in the world meteorite collection are comparable. It seems too much of a coincidence if several meteorites with the same unique composition were from different fall events but are geographically on an array. This strongly suggests that all the Aletai masses are from the same fall event.

We consider that the breakup of asteroid Aletai and the formation of the long Aletai strewn field could not result from a crater-forming process like what Canyon Diablo experienced (i.e., impact fragmentation and ejection) (*29*) for the following reasons: (i) There is no crater reported in Aletai area. Although a 3.6-km Tsenkher Crater has been reported in the Gobi-Altai region of Mongolia, it seems to be unrelated to Aletai because of its relatively old formation age [^{40}Ar-^{39}Ar impact age of ~5 Ma for Tsenkher Crater versus buried Aletai irons in Quaternary sediments (<2.58 Ma)] and long-distance (~370 km) away from the long axis of Aletai strewn field (*30*). (ii) The distance between 18-ton Akebulake and 0.43-ton Ulasitai is too long (~430 km). If Aletai meteorites are solid fragments of impactors that are ejected, then the northwest end of this strewn field, where more than half of the total mass is concentrated (i.e., adjacent to Xiaodonggou area), is most likely to be the first contact site. Nevertheless, the 0.43-ton mass launched from the surface has a maximum flight distance of ~90 km (ejection velocity of 0 to 7.5 km/s, ejection angle of 0° to 90°, and ablation of minor importance; Eqs. 1 to 8), inconsistent with the ~430-km-long separation between Akebulake and Ulasitai. In this regard, the breakup of Aletai most likely happened before hitting the ground.

Fragments could be broken up from their parent meteoroids/asteroids before entering into the atmosphere, such as the Shoemaker–Levy 9 impact on Jupiter (*31*). The same scenario was also invoked for the Chant Meteor Procession of 1913 (*32*). Tidal force may disintegrate fragile asteroids (e.g., comets and loosely attached stony asteroid) into fragments (*33*); however, it appears unlikely to disrupt a small 2 to 20-m single iron body (a few pascals for tidal strength versus a few million pascals for tensile strength), although the structure of M-type asteroid (i.e., rubble pile or monolithic) is still poorly known. Rigorously speaking, we cannot fully exclude the possibility of a multiple-fragment entry scenario (i.e., breakup before entering into the atmosphere). Nonetheless, to consider the multiple-fragment entry scenario, more parameters (e.g., the distance between different fragments) would be introduced on the basis of numerous additional assumptions, which is outside the scope of this study. In this study, we only focus on the widely used single-body entry model (*34*).

Our modeling results show that asteroid Aletai breaks into several fragments in the atmosphere. This conforms to (i) the existence of unsmoothed "torn surface" on Armanty that was inferred to have formed during fragmentation at a relatively low altitude (fig. S5) (*12*) and (ii) the heterogeneous internal structure of pre-atmospheric asteroid Aletai as indicated by the varying degrees of shock metamorphism between different masses. As shown by the representative case in Fig. 4, the estimated length of strewn field is basically comparable with that of the currently known Aletai strewn field, although it could be up to 1000 km in some cases. Also, in accordance with the scarcity of impact craters in the Aletai area, the modeling results show relatively low impact energy on Earth's surface (e.g., ~1 to 8 t TNT for the largest mass). Some unexpected large masses occurring along the modeled strewn field imply that more masses are possibly to be found in the future. There is one major difference between modeling and observation: Our modeling results generally show one single large mass (~50 tons) in the farthest end of strewn field, while the northwest end of Aletai strewn field contains several large masses (5 to 23 tons; >46 tons in total). This suggests that a subsequent disintegration in the farthest end is not reflected by our modeling. In numerical modeling, fragmentation is assumed to take place whenever the dynamic pressure exceeds the calculated strength (Eqs. 9 and 10). Nevertheless, fragmentation process is much more complex in reality, which is indicated by the records of observed meteorite falls. Although later fragmentation generally takes place under higher dynamic pressure corresponding to higher meteoritic strength (consistent with the Weibull statistics) (*35*), some meteorites (e.g., Morávka meteorite) did show that later fragmentation could have slightly lower dynamic pressure (e.g., ~3 to 5 MPa for later fragmentation versus ~5 MPa for earlier fragmentation) (*36*). This could be caused by increasing thermal stress (*36*) or local low strength because of the uneven distribution of fractures. In this regard, we suggest that further disintegration of Aletai in the farthest end of this strewn field could be caused by the heterogeneous internal structure of Aletai. If the later breakup did happen, then the dynamic pressure at breakup could be ~1 to 3 MPa (fig. S4), slightly lower than the earlier fragmentation (~3 to 4 MPa). Although lacking data from iron falls for comparison, the estimated dynamic pressure at breakup (i.e., ~1 to 3 MPa for later breakup) is higher than most stony meteoroids (~0.1 to 1 MPa) but slightly lower than some strong meteoroids (~3 to 10 MPa) (*35*, *37*), which seems to be within a reasonable range.

Most meteoroids/asteroids enter Earth's atmosphere at an entry angle interval of 30° to 60° (*38*). They generally have a relatively short flight distance, which would lead to a relatively small strewn field. In contrast, the low entry angle makes a difference. Except for rare cases (e.g., meteoroid Peekskill) that fell on the Earth after deceleration (*39*, *40*), almost all meteoroids/asteroids with an extremely shallow entry angle either were fully ablated or escaped from Earth after traveling through the atmosphere [e.g., 1972 grazing fireball (*41*)]. In the case of Aletai, the low entry angle (~6.5° to 7.3°) could contribute to the formation of the long strewn field with a unique stone skipping–like trajectory. The parameter range (e.g., initial velocity, entry angle, and initial mass), calculated from MCMC method for reference, is mainly based on current observations. We should stress that our modeling results may change with the further recovery of new masses in future. Even so, although the recovery of unidentified masses could extend the length of strewn field and increase the total mass, Aeltai's stone skipping–like trajectory would not change if the single-body entry scenario is considered. The stone skipping–like trajectory could be the result of direct entry; alternatively, recent numerical modeling suggested that meteoroids could be captured into Earth's orbit [e.g., temporarily captured obiters (*42*)] and reenter Earth's atmosphere more than once with the stone skipping–like trajectory in the final entry (*43*). Although such a shallow entry angle results in the deposition of relatively low impact energy on Earth's

surface, it could lead to the dissipation of energy in the atmosphere. This could cause influences across fairly broad areas during its extremely long-distance flight.

To the best of our knowledge, such a stone skipping–like trajectory has not been reported for any falls or finds in the nature. It is possible that some ancient meteoroids/asteroids with stone skipping–like trajectories failed to be identified. Some meteoroids/asteroids could be resistant to breakup during the long-distance traveling in the atmosphere. Alternatively, some masses recovered at long separation distances may fail to be paired since they are not uncommon in chemistry or suspected to be artificially transported in cases of small masses. The identification of the unique stone skipping–like trajectory for asteroid Aletai mainly benefits from its unique geochemical characteristics (IIIE-an in composition) and the long separation distances between massive masses.

MATERIALS AND METHODS

Experimental design

To study Aletai's petrographic, mineralogical and geochemical characteristics, electron microscope, and electron probe analysis were performed for Akebulake and WuQilike mass, and whole-rock trace elemental analysis was conducted for Armanty, Akebulake, Wuxilike, and Ulasitai mass. Integrated with radionuclides analysis, numerical modeling was performed to study the dynamics and trajectory of asteroid Aletai. The details are as follows.

Petrographic studies

Two slices of Akebulake (332 and 435 mm^2, respectively) and one slice of WuQilike (223 mm^2) were made into 1-inch round thick sections. Kamacite bandwidths were measured under a stereo-optical microscope with an uncertainty of 0.2 mm. Petrographical observation was performed using a Hitachi S-3400N II scanning electron microscope equipped with an Oxford X-Max 20 energy dispersive spectroscope at Purple Mountain Observatory (PMO).

Mineral major element analysis

Opaque mineral compositions were characterized with the JEOL JXA-8230 electron microprobe at PMO using an acceleration voltage of 20 kV, a 20-nA sample current, and a focused beam with spot analysis. The measurement times for elemental peak and background are 20 and 10 s, respectively. The standards are indium phosphide for P, pyrite for S, bustamite for Mn, and 99.99% pure-iron, cobalt, nickel, chromium, and copper metal for Fe, Co, Ni, Cr, and Cu, respectively. The Co concentrations in metallic Fe-Ni grains were corrected for the overlap of the Fe-Kß peak on the Co-Kα peak after analyzing a 99.99% iron standard. Data were processed with the conventional ZAF method. Detection limits are ~0.01 wt % for all the elements.

Whole-rock compositions

Bulk compositions of four Aletai masses (Akebulake, Armanty, Wuxilike, and Ulasitai) were reanalyzed by J.T. Wasson at University of California, Los Angeles. The detailed INAA procedure was described by Wasson (*21*, *22*). Sixteen elements (15 plus Fe) in metal were determined in replicate analyses, and data of Fe were applied for internal normalization. Relative 95% confidence limits on the means are estimated to be 1.5 to 3% for Co, Ni, Ga, Ir, and Au; 4 to 6% for As; and 7 to 10% for Cu, Ru (values of >2 μg/g), W, and Pt. Stibium, Re, Os, and Ge contents are below the INAA detection limit and not listed in table S4 (detection limit: Re: ~40 ng/g; Sb: ~150 ng/g; Ge: ~50 μg/g; Os: ~2 μg/g).

Analysis of radionuclides

Analyses of ^{10}Be for Wuxilike and Akebulake were conducted at the University of Arizona Accelerator Mass Spectrometry Laboratory. Samples (~0.1 g) dissolved in HF-HNO_3 were first mixed with 0.3 mg of $Be(OH)_2$. Beryllium was separated by a combination of acetyl acetone extraction and ion chromatography. $^{10}Be/^{9}Be$ ratios were normalized to the National Institute of Standards and Technology standard with an isotopic ratio of 2.79×10^{-11}. The detailed procedure was described by Jull *et al.* (*44*).

Numerical models for dynamics

We assume that asteroid Aletai is spherical in shape, and the simulation begins at an altitude of 100 km. The lift and side forces are ignored in this study. The dynamics in the atmosphere is described under the planar reference frame over a nonrotating Earth by the following equations (*45*, *46*)

$$\frac{dh}{dt} = v\sin\theta \tag{1}$$

$$\frac{dv}{dt} = -\frac{1}{2}C_d\rho_a v^2 A/m - g\sin\theta \tag{2}$$

$$\frac{d\theta}{dt} = \cos\theta\left(\frac{v}{R_E + h} - \frac{g}{v}\right) \tag{3}$$

$$\frac{dm}{dt} = -\frac{1}{2}\rho_a v^3 AC_{ab} \tag{4}$$

$$\frac{d\zeta}{dt} = \frac{v\cos\theta}{R_E + h} \tag{5}$$

$$g = g_0\left(\frac{R_E}{R_E + h}\right)^2 \tag{6}$$

$$\rho_a = \rho_0 e^{-h/H} \tag{7}$$

$$FD = \zeta R_E \tag{8}$$

where h is the altitude, t is the time from atmospheric entry point, v is the velocity of object, θ is the flight path angle, g is the gravitational acceleration [(g_0 ~ 9.81 m/s^2 and earth radius (R_E) ~ 6.371×10^6 m; Eq. 6], A is the cross-sectional area, m is the object mass, ρ_a is the atmospheric density in an exponential atmosphere model [reference atmospheric density at sea level (ρ_0) ~ 0.00129 g/cm^3 and atmospheric scale height (H) ~ 7160 m; Eq. 7], C_d is the constant drag coefficient (~1), C_{ab} is the ablation coefficient, ζ is the angular range distance calculated from the atmospheric entry point, and *FD* is the flight distance.

The internal strength of a meteoroid/asteroid complies with Weibull statistics

$$\sigma = \sigma_0\left(\frac{m_0}{m}\right)^a \tag{9}$$

where m_0 is the mass of a reference sample, σ_0 is the strength of a reference sample, a is an exponential strength scaling factor, σ is the strength of the studied body, and m is the mass of the studied body. A meteoroid/asteroid would begin to disrupt into fragments whenever its strength is lower than the dynamic pressure (*47*, *48*). The mass of separated fragments is a random choice. The equation of dynamic pressure is expressed by

$$p = \rho_a v^2 \quad (10)$$

where ρ_a is atmospheric density and v is meteoroid/asteroid velocity as those in Eqs. 1 to 8. The lateral velocity is not considered in the model.

The iron has a density of 7800 kg/m^3 (*49*). The reported strength values of iron meteorites (different sizes) are between ~44 and 440 MPa (*48*, *50*). Here, the tensile strength of 44 MPa from the well-studied Sikhote-Alin iron (1-kg sample) is adopted (*48*). The ablation coefficient C_{ab} and strength scaling factor α vary over a wide range (0.01 to 0.07 s^2/km^2 for C_{ab} and ~0.1 to 0.5 for a), depending on the physical properties of specific meteoroids/asteroids (*6*, *35*, *51*). For numerical modeling, they are searched in a multidimensional parameter space to explore the optimal values that best produce the observed Aletai strewn field. Here, a value of 0.02 s^2/km^2 is used for C_{ab}, and a value of 0.2 is set for a.

First, we perform a three-dimensional Monte Carlo model with 30,000 samplings to obtain a general view of asteroid entry scenario and test the ranges of input parameters. The three main input parameters are the entry angle (θ_i, 4° to 10°), initial velocity (v_i, 11.2 to 20 km/s), and initial mass (m_i, 200 to 20,000 tons). Then, we use a Metropolis-Hastings MCMC algorithm to modal the parameters ω including three elements v_i, m_i, and θ_i. The MCMC sampler searches in the following parameter space: $11.2\,\mathrm{km/s} \le v_i \le 20\,\mathrm{km/s}$; $5^\circ \le \theta_i \le 85^\circ$; $200\,\mathrm{tons} \le m_i \le 20{,}000\,\mathrm{tons}$. The posterior probability density can be obtained via Bayes' theorem

$$P_{\mathrm{post}}(\omega \mid Y) \propto L \cdot P_{\mathrm{prior}}(\omega) \quad (11)$$

where L is likelihood function, P_{post} is the posterior probability density function, and P_{prior} is the uniform prior probability density function.

The likelihood function can be expressed as

$$L = \prod_{i=1}^{n} P(Y_i \mid \omega) \quad (12)$$

and the corresponding log-likelihood function is

$$\ln L = \sum_{i=1}^{n} \ln P(Y_i \mid \omega) \quad (13)$$

In Eqs. 12 and 13, Y_i is the i - th modeling strewn field parameter and n is the number of measurements. The observed and modeling parameters of the strewn field (Y) include (i) the maximum weight of the single final fragment, (ii) the longest separation between large fragments (individual mass > 20 tons), and (iii) the number of large fragments (individual mass > 20 tons). It is assumed that the strewn field parameters obey a Gaussian distribution except that the number of large masses (>20 tons individually) follows a Poisson distribution. We assume that (i) the maximum weight of the single final fragment is 50 (σ = 10), (ii) the longest separation between large fragments (individual mass > 20 tons) is 300 (σ = 50), and (iii) the number of large fragments (individual mass > 20 tons) is 2. The assumption (i) is adopted in terms of Monte Carlo method–based preliminary studies, which shows that large mass in the farthest end of a long strewn field (>430 km) generally occurs as one single fragment without further fragmentation (see Discussion for more details). Thus, the total weight (>46 tons) in the northwest end of this strewn field is used to constrain the maximum mass of the single final fragment. We do not constrain the total length of the strewn field, assuming that more fragments are likely to be found.

We run about 2000 interactions and obtain 7200 samples of posterior distribution. The first 500 interactions are discarded as burn-in. A publicly available Interactive Data Language code is used for MCMC modeling (*52*). The detailed method description refers to Metropolis *et al.* (*53*) and Hastings (*54*).

SUPPLEMENTARY MATERIALS

Supplementary material for this article is available at https://science.org/doi/10.1126/sciadv.abm8890

REFERENCES AND NOTES

1. N. Gorkavyi, A. Dudorov, S. Taskaev, *Chelyabinsk Superbolide* (Springer, 2019).
2. M. Bronikowska, N. A. Artemieva, K. Wünnemann, Reconstruction of the Morasko meteoroid impact—Insight from numerical modeling. *Meteorit. Planet. Sci.* **52**, 1704–1721 (2017).
3. G. O. Ryabova, D. J. Asher, M. J. Campbell-Brown, *Meteoroids: Sources of Meteors on Earth and Beyond* (Cambridge Univ. Press, 2019).
4. P. Schulte, L. Alegret, I. Arenillas, J. A. Arz, P. J. Barton, P. R. Bown, T. J. Bralower, G. L. Christeson, P. Claeys, C. S. Cockell, G. S. Collins, A. Deutsch, T. J. Goldin, K. Goto, J. M. Grajales-Nishimura, R. A. Grieve, S. P. Gulick, K. R. Johnson, W. Kiessling, C. Koeberl, D. A. Kring, K. G. MacLeod, T. Matsui, J. Melosh, A. Montanari, J. V. Morgan, C. R. Neal, D. J. Nichols, R. D. Norris, E. Pierazzo, G. Ravizza, M. Rebolledo-Vieyra, W. U. Reimold, E. Robin, T. Salge, R. P. Speijer, A. R. Sweet, J. Urrutia-Fucugauchi, V. Vajda, M. T. Whalen, P. S. Willumsen, The Chicxulub asteroid impact and mass extinction at the Cretaceous-Paleogene boundary. *Science* **327**, 1214–1218 (2010).
5. O. P. Popova, P. Jenniskens, V. Emel'yanenko, A. Kartashova, E. Biryukov, S. Khaibrakhmanov, V. Shuvalov, Y. Rybnov, A. Dudorov, V. I. Grokhovsky, D. D. Badyukov, Q.-Z. Yin, P. S. Gural, J. Albers, M. Granvik, L. G. Evers, J. Kuiper, V. Kharlamov, A. Solovyov, Y. S. Rusakov, S. Korotkiy, I. Serdyuk, A. V. Korochantsev, M. Y. Larionov, D. Glazachev, A. E. Mayer, G. Gisler, S. V. Gladkovsky, J. Wimpenny, M. E. Sanborn, A. Yamakawa, K. L. Verosub, D. J. Rowland, S. Roeske, N. W. Botto, J. M. Friedrich, M. E. Zolensky, L. Le, D. Ross, K. Ziegler, T. Nakamura, I. Ahn, J. I. Lee, Q. Zhou, X.-H. Li, Q.-L. Li, Y. Liu, G.-Q. Tang, T. Hiroi, D. Sears, I. A. Weinstein, A. S. Vokhmintsev, A. V. Ishchenko, P. Schmitt-Kopplin, N. Hertkorn, K. Nagao, M. K. Haba, M. Komatsu, T. Mikouchi; Chelyabinsk Airburst Consortium, Chelyabinsk airburst, damage assessment, meteorite recovery, and characterization. *Science* **342**, 1069–1073 (2013).
6. V. V. Svetsov, I. V. Nemtchinov, A. V. Teterev, Disintegration of large meteoroids in Earth's atmosphere: Theoretical models. *Icarus* **116**, 131–153 (1995).
7. G. S. Collins, H. J. Melosh, R. A. Marcus, Earth impact effects program: A web-based computer program for calculating the regional environmental consequences of a meteoroid impact on Earth. *Meteorit. Planet. Sci.* **40**, 817–840 (2005).
8. M. H. Shaddad, P. Jenniskens, D. Numan, A. M. Kudoda, S. Elsir, I. F. Riyad, A. Ali, E. M. Alameen, N. M. Alameen, O. Eid, A. T. Osman, M. I. Abubaker, M. Yousif, S. R. Cheseley, P. W. Chodas, J. Albers, W. N. Edwards, P. Brown, J. Kuiper, J. M. Friedrich, The recovery of asteroid 2008 TC$_3$. *Meteorit. Planet. Sci.* **45**, 1557–1589 (2010).
9. A. Bouvier, J. Gattaceaca, J. Grossman, K. Metzler, The Meteoritical Bulletin, No. 105. *Meteorit. Planet. Sci.* **52**, 2411 (2016).
10. K. C. Wang, W. B. Hsu, Aletai: The longest meteorite strewn field on Earth. *Chin. Sci. Bull.* **61**, 2834–2842 (2016).
11. Y. Chen, D. Wang, Mineralogical features of Xinjiang iron meteorite and forming conditions of its parent body (in Chinese). *Acta Mineral. Sinica* **9**, 119–125 (1989).
12. J. T. Wasson, X. W. Ouyang, D. D. Wang, Compositional study of a suite of samples from the 28-t Armanty (Xinjiang) iron meteorite. *Meteoritics* **23**, 365–369 (1988).
13. L. Xu, B. Miao, Y. Lin, Z. Ouyang, Ulasitai: A new iron meteorite likely paired with Armanty (IIIE). *Meteorit. Planet. Sci.* **43**, 1263–1273 (2008).
14. M. C. L. Rocca, A catalogue of large meteorite specimens from Campo del Cielo meteorite shower, Chaco province, Argentina. *Meteorit. Planet. Sci.* **41**, 5001 (2006).
15. E. Flamini, M. D. Martino, A. Coletta, Campo del Cielo, Argentina, in *Encyclopedic Atlas of Terrestrial Impact Craters* (Springer, 2019), pp. 657–658.
16. V. F. Buchwald, *Handbook of Iron Meteorites* (University of California Press, 1975).
17. Y. H. Mao, "Determination of metallographic cooling rate of meteorites and study of thermal history of their parent bodies (in Chinese)," thesis, Guangzhou Institute of Geochemistry, CAS, Guangzhou (1998).
18. J. A. Wood, The cooling rates and parent planets of several iron meteorites. *Icarus* **3**, 429–459 (1964).
19. J. P. Breen, A. E. Rubin, J. T. Wasson, Variations in impact effects among IIIE iron meteorites. *Meteorit. Planet. Sci.* **51**, 1611–1631 (2016).

20. N. Sugiura, Y. Ikeda, S. Zashu, J. T. Wasson, Nitrogen-isotopic compositions of IIIE iron meteorites. *Meteorit. Planet. Sci.* **35**, 749–756 (2000).
21. J. T. Wasson, Formation of non-magmatic iron-meteorite group IIE. *Geochim. Cosmochim. Acta* **197**, 396–416 (2017).
22. J. T. Wasson, Campo del Cielo: A Campo by any other name. *Meteorit. Planet. Sci.* **54**, 280–289 (2019).
23. T. Smith, D. L. Cook, S. Merchel, S. Pavetich, G. Rugel, A. Scharf, I. Leya, The constancy of galactic cosmic rays as recorded by cosmogenic nuclides in iron meteorites. *Meteorit. Planet. Sci.* **54**, 2951–2976 (2019).
24. N. Shankar, G. Rugel, T. Faestermann, G. Korschinek, C. C. Swisher III, B. Turrin, G. F. Herzog, R. J. Walker, ^{10}Be, ^{26}Al, and ^{36}Cl in iron meteorites: Implications for osmium isotope systematics, in *Lunar and Planetary Science Conference XLII* (2011), pp. 1262.
25. K. Ammon, I. Leya, Y. Lin, Noble gases in the Xinjiang (Armanty) iron meteorite—A big object with a short cosmic-ray exposure age. *Meteorit. Planet. Sci.* **46**, 785–792 (2011).
26. E. R. D. Scott, J. T. Wasson, V. F. Buchwald, The chemical classification of iron meteorites—VII. A reinvestigation of irons with Ge concentrations between 25 and 80 ppm. *Geochim. Cosmochim. Acta* **37**, 1957–1983 (1973).
27. D. J. Malvin, D. Wang, J. T. Wasson, Chemical classification of iron meteorites—X. Multielement studies of 43 irons, resolution of group IIIE from IIIAB, and evaluation of Cu as a taxonomic parameter. *Geochim. Cosmochim. Acta* **48**, 785–804 (1984).
28. J. T. Wasson, B.-G. Choi, E. A. Jerde, F. Ulff-Møller, Chemical classification of iron meteorites: XII. New members of the magmatic groups. *Geochim. Cosmochim. Acta* **62**, 715–724 (1998).
29. D. Heymann, M. E. Lipschutz, B. Nielsen, E. Anders, Canyon Diablo meteorite: Metallographic and mass spectrometric study of 56 fragments. *J. Geophys. Res.* **71**, 619–641 (1966).
30. G. Komatsu, J. Ormö, T. Bayaraa, T. Arai, K. Nagao, Y. Hidaka, N. Shirai, M. Ebihra, C. Alwmark, L. Gereltsetseg, S. Tserendug, K. Goto, T. Matsui, S. Demberel, Further evidence for an impact origin of the Tsenkher structure in the Gobi-Altai, Mongolia: Geology of a 3.7 km crater with a well-preserved ejecta blanket. *Geol. Mag.* **156**, 1–24 (2019).
31. J. C. Solem, Density and size of comet Shoemaker–Levy 9 deduced from a tidal breakup model. *Nature* **370**, 349–351 (1994).
32. M. Beech, M. Comte, The chant meteor procession of 1913 – Towards a descriptive model. *Am. J. Astron. Astrophys.* **6**, 31–38 (2018).
33. E. Schunová, R. Jedicke, K. J. Walsh, M. Granvik, R. J. Wainscoat, N. Haghighipour, Properties and evolution of NEO families created by tidal disruption at Earth. *Icarus* **238**, 156–169 (2014).
34. Z. Ceplecha, D. O. Revelle, Fragmentation model of meteoroid motion, mass loss, and radiation in the atmosphere. *Meteorit. Planet. Sci.* **40**, 35–54 (2005).
35. O. Popova, J. Borovička, W. K. Hartmann, P. Spurný, E. Gnos, I. Nemtchinov, J. M. Trigo-Rodríguez, Very low strengths of interplanetary meteoroids and small asteroids. *Meteorit. Planet. Sci.* **46**, 1525–1550 (2011).
36. J. Borovička, P. Kalenda, The Morávka meteorite fall: 4. Meteoroid dynamics and fragmentation in the atmosphere. *Meteorit. Planet. Sci.* **38**, 1023–1043 (2003).
37. O. Popova, Meteoroid ablation models. *Earth Moon Planets* **95**, 303–319 (2004).
38. D. W. Hughes, Meteorite incidence angles. *J. Br. Astron. Assoc.* **103**, 123–126 (1993).
39. P. M. Shober, T. Jansen-Sturgeon, E. K. Sansom, H. A. R. Devillepoix, M. C. Towner, P. A. Bland, M. Cupák, R. M. Howie, B. A. D. Hartig, Where did they come from, where did they go: Grazing fireballs. *Astrophys. J.* **159**, 191 (2020).
40. P. Brown, Z. Ceplecha, R. L. Hawkes, G. Wetherill, M. Beech, K. Mossman, The orbit and atmospheric trajectory of the Peekskill meteorite from video records. *Nature* **367**, 624–626 (1994).
41. R. D. Rawcliffe, C. D. Bartky, F. Li, E. Gordon, D. Carta, Meteor of August 10, 1972. *Nature* **247**, 449–450 (1974).
42. R. Jedicke, B. T. Bolin, W. F. Bottke, M. Chyba, G. Fedorets, M. Granvik, L. Jones, H. Urrutxua, Earth's Minimoons: Opportunities for science and technology. *Front. Astron. Space Sci.* **5**, 13 (2018).
43. S. Geng, B. Zhou, M. Li, On the capture of small stony asteroids into the Earth's orbit by atmospheric grazing. *Mon. Not. R. Astron. Soc.* **507**, 4661–4668 (2021).
44. A. J. T. Jull, L. R. McHargue, P. A. Bland, R. C. Greenwood, A. W. R. Bevan, K. J. Kim, S. E. LaMotta, J. A. Z. Johnson, Terrestrial ages of meteorites from the Nullarbor region, Australia, based on ^{14}C and ^{14}C-^{10}Be measurements. *Meteorit. Planet. Sci.* **45**, 1271–1283 (2010).
45. S. Limonta, M. Trisolini, S. Frey, C. Colombo, Fragmentation model and strewn field estimation for meteoroids entry. *Icarus* **367**, 114553 (2021).
46. P. J. Register, D. L. Mathias, L. F. Wheeler, Asteroid fragmentation approaches for modeling atmospheric energy deposition. *Icarus* **284**, 157–166 (2017).
47. N. A. Artemieva, V. V. Shuvalov, Interaction of shock waves during the passage of a disrupted meteoroid through the atmosphere. *Shock Waves* **5**, 359–367 (1996).
48. N. A. Artemieva, V. V. Shuvalov, Motion of a fragmented meteoroid through the planetary atmosphere. *J. Geophys. Res.* **106**, 3297–3309 (2001).
49. P. Bland, N. A. Artemieva, The rate of small impacts on Earth. *Meteorit. Planet. Sci.* **41**, 607–631 (2006).
50. R. Knox Jr., The yield strength of meteoritic iron. *Meteoritics* **5**, 63–74 (1970).
51. D. O. ReVelle, Z. Ceplecha, Analysis of identified iron meteoroids: Possible relation with M-type Earth-crossing asteroids? *Astron. Astrophys.* **292**, 330–336 (1994).
52. J. M. Zobitz, A. R. Desai, D. J. P. Moore, M. A. Chadwick, A primer for data assimilation with ecological models using Markov Chain Monte Carlo (MCMC). *Oecologia* **167**, 599–611 (2011).
53. N. Metropolis, A. W. Rosenbluth, M. N. Rosenbluth, A. H. Teller, E. Teller, Equation of state calculations by fast computing machines. *J. Chem. Phys.* **21**, 1087–1092 (1953).
54. W. K. Hastings, Monte Carlo sampling methods using Markov chains and their applications. *Biometrika* **57**, 97–109 (1970).
55. N. L. Chabot, B. D. Zhang, A revised trapped melt model for iron meteorites applied to the IIIAB group. *Meteorit. Planet. Sci.* **57**, 200–227 (2021).
56. A. Guy, K. Schulmann, I. Soejono, W. J. Xiao, Revision of the Chinese Altai-East Junggar terrane accretion model based on geophysical and geological constraints. *Tectonics* **39**, e2019TC006026 (2020).
57. S. Zhou, J. Li, J. Zhao, J. Wang, J. Zheng, Quaternary glaciations: Extent and chronology in China, in *Developments in quaternary sciences*, J. Elhers, P. Gibbard, P. D. Hughes, Eds. (Elsevier, 2011), vol. 15, pp. 981–1002.
58. J. I. Goldstein, G. R. Huss, E. R. D. Scott, Ion microprobe analyses of carbon in Fe-Ni metal in iron meteorites and mesosiderites. *Geochim. Cosmochim. Acta* **200**, 367–407 (2017).
59. E. R. D. Scott, J. I. Goldstein, Occurrence of carbides and graphite in iron meteorites and origin of C-rich irons, in *Lunar and Planetary Science Conference XLIII* (2012), pp. 2671.
60. R. S. Clarke Jr., J. I. Goldstein, Schreibersite growth and its influence on the metallography of coarse-structured iron meteorites. *Smithsonian Contrib. Earth Sci.* **21**, 1–80 (1978).
61. E. R. D. Scott, Origin of rapidly solidified metal-troilite grains in chondrites and iron meteorites. *Geochim. Cosmochim. Acta* **46**, 813–823 (1982).

Acknowledgments: This work is dedicated to J. T. Wasson who performed INAA analysis of Aletai irons and made a notable contribution during the earliest stage of manuscript preparation. If J. T. Wasson had the opportunity to read this manuscript, it would have been in a better shape. We thank the three anonymous reviewers and journal editors for thoughtful and constructive suggestions and comments. We are very grateful to Z.Y. Xiao for advice and helpful discussions. Assistance and suggestions from K. Wang, Y. Wang, L.L. Pan, S.C. Hu, and L. Yao are highly appreciated. **Funding:** W.H. thanks the B-type Strategic Priority Program of the Chinese Academy of Sciences (grant no. XDB41000000), the pre-research Project on Civil Aerospace Technologies (grant nos. D020202 and D020302), the opening fund of State Key Laboratory of Lunar and Planetary Sciences, Macau University of Science and Technology (Macau FDCT grant nos. 119/2017/A3 and 0111/2020/A), the National Key Research and Development Program of China (2021YFA0716100), and the National Natural Science Foundation of China (grant no. 41973060) for supporting. Y.L. acknowledges the National Natural Science Foundation of China (grant no. 41803051) for supporting. B.L. and H.Z. thank the National Natural Science Foundation of China (grant no.11633009), Civil Aerospace pre-research project (no. D020304), and Space debris and NEO research project (nos. KJSP2020020204 and KJSP2020020102). S.L. is supported by the National Natural Science Foundation of China (grant no. 42073060). W.H., Y.L., B.L., S. Liao, Y.Z., and H.Z. also thank the Minor Planet Foundation of China. A.J.T.J. acknowledges support from the European Union and the State of Hungary, co-financed by the European Regional Development Fund project no. GINOP-2.3.2-15-2016-00009 ICER. **Author contributions:** Y.L. and B.L. contributed equally to this manuscript and, therefore, are listed as co-first authors. Y.L. and W.H. designed the project and wrote the manuscript; B.L. performed numerical modeling and interpreted the calculated results; A.J.T.J. obtained and interpreted the ^{10}Be data; Y.L., W.H., S. Liao, Y.Z., H.Z., S. Li, Y.W., and C.T. interpreted the data. All authors contributed to the preparation of the manuscript. **Competing interests:** The authors declare that they have no competing interests. **Data and materials availability:** All data needed to evaluate the conclusions in the paper are present in the paper and/or the Supplementary Materials. Aletai meteorite samples are available upon request.

Submitted 19 October 2021
Accepted 9 May 2022
Published 24 June 2022
10.1126/sciadv.abm8890